C-Band FMCW radar based on SDR system generation and 2D-MLBI reception for UAV detection and tracking

Salvador Andres[(1)], Jorge Lanzuela[(1)], Andres Ocabo[(1)], Asier Villafranca[(1)], Iñigo Salinas[(2)], Rafael Alonso[(2)], Carlos Heras [(2)]
salva@zepren.com, jlanzuela@zepren.com, aocabo@zepren.com, asier@zepren.com, isalinas@unizar.es, ralonso@unizar.es, cdheras@unizar.es.
[(1)] Dept. of R&D. ZEPREN Solutions S.L. C/ María Luna, 11, 50018, Zaragoza
(2) Aragon Institute of Eng. Res(I3A). Universidad de Zaragoza. C/Mariano Esquillor Gomez, 3, 50018, Zaragoza.

***Abstract*— This paper presents a frequency modulation continuous wave (FMCW) C-band radar system with high sensitivity and 2D detection capacity to detect low-radar cross section targets and to measure their range and velocity. A low jitter high signal-to-noise and distortion ratio (SINAD) S band signal is directly generated by an SDR system which greatly increases the quality of the obtained and measured signals. Up conversion to C-Band by x2 frequency multiplication is performed. Proper amplification and filtering of emitted and detected signals are implemented to achieve 70dB dynamic range in the final system. The transmitter antenna is a single 60º aperture whereas multi-long baseline interferometer (MLBI) concept is implemented in the receiver antenna for a low cost, low dimension, and high angle resolution in the 2D position of the targets. Measurements in terms of the range and the velocity of a small drone have been carried out to evaluate the proposed radar system. Micro-Doppler signature is also measured and evaluated. The results show that we can clearly detect, identify and track the small drone within a 350 m range, which demonstrates the high performance of the radar and its potential use for unmanned aerial vehicles (UAV) tracking and identification.**

I. INTRODUCTION

FMCW homodyne systems have been extensively studied and have been widely used for a variety of applications, including range and velocity estimations [1-2]. It is widely acknowledged that frequency sweep nonlinearity can often limit radar performance [3].

In this way, software-defined radio (SDR) systems offer an opportunity to address some of these issues. SDR implementation provides high bandwidth (BW) with low jitter, resulting in improved range and velocity accuracy estimation [4]. Additionally, the estimation of target angle position has been well resolved in both 2D and 3D using beamforming techniques and tracking strategies have been well established in the literature [5]. Notably, the high cost of certain applications can limit their use. In recent years, based on the multi-long baseline interferometer (MLBI) concept, new and cheaper strategies for estimating the angle of arrival (AOA) of active targets have been developed [6]. These techniques are not tested yet on radar systems.

This work describes the implementation of a C-band homodyne FMCW radar system using SDR hardware to generate a low-jitter, high-SINAD signal, and a 3-element MLBI receiver for 2D detection and tracking. The achieved signal quality allows for the detection and ranging of low-radar cross-section (RCS) UAVs, up to 350m, including the measurement of their 2D trajectory and velocity. Further, high quality of the achieved signals allows the study of micro-Doppler signatures (MDS) for target characterization [7].

The final performance of the radar system was assessed in a controlled open field test, using a DJI Mavic 3 for distances of up to 350m. The results indicate that this radar concept has potential for medium-cost applications.

II. BASIC THEORETICAL CONCEPTS

The FMCW radar utilizes a continuous wave signal with linear frequency modulation from the starting frequency, f_0, up to $f_0 + BW$ during the chirp time t_c, as it is detailed in Eq.1. The resulting transmitted signal, S_{Tx}, is described in Eq.2.

$$f_{chrip} = f_0 + \frac{BW}{t_c} \cdot t \tag{1}$$

$$S_{Tx} = A_{Tx} sin\left[2\pi\left(f_0 t + \frac{\mathrm{BW}}{2t_c}\mathrm{t}^2 + \phi_{\mathrm{Tx}}\right)\right] \tag{2}$$

where ϕ_{Tx} is the initial phase, A_{Tx} is the amplitude of the transmitted signal and t the time elapsed since the wave emission. The received target echo signal S_{Rx} is a reflected, attenuated and time delayed copy of the transmitted signal. The time delay τ of the received signal depends on the target speed, v_r, and its original position, R_0, as shown in Eq.3. Eq.4 gives the received signal.

$$\tau = \frac{2\mathrm{R}_0}{c} + \frac{2v_r t}{c} \tag{3}$$

$$S_{Rx}=A_{Rx} sin\left\{2\pi\left[f_0(t-\tau) + \frac{\mathrm{BW}}{2t_c}(\mathrm{t}-\tau)^2 + \phi_{\mathrm{Rx}}\right]\right\} \tag{4}$$

where ϕ_{Rx} is the phase, A_{Rx} is the amplitude of the received signal and c is the light speed.

In the homodyne architecture, the received signal is combined with the transmitted signal to generate a new not chirped sinusoid signal known as beat frequency signal, S_{beat}. The resulting signal is described by Eq.5.

$$S_{beat} = \mathrm{G} \cdot A_{Rx} sin[2\pi(f_b t + \phi_{beat})] \tag{5}$$

with G the system gain, ϕ_{beat} is the beat frequency signal phase, f_b is the beat frequency.

According to Eq. 6, the frequency difference between the transmitted and received signals is proportional to the slope of

the chirped frequency, BW/t_c, and the time delay of the received signal, $2R_0/c$. Additionally, Eq. 7 describes how the phase shift of the received signal, denoted by ϕ_{beat}, is dependent on both the R_0 and the phase shift due to the reflection properties of the target, denoted by κ.

$$f_b = 2\frac{v_r}{\lambda} + \frac{BW \cdot 2 \cdot R_0}{t_c \cdot c} = f_D + f_R \quad (6)$$

$$\phi_{beat} = 2 \cdot \frac{R_0}{\lambda} + \kappa \quad (7)$$

Where λ is the mean wavelength of the chirp signal.

The beat frequency is composed of two components: the doppler frequency f_D and the range frequency f_R. Note that during the chirp duration, the doppler frequency term is insignificant. However, in subsequent chirps, which are referred to as a chirp frame, the doppler term increases enough to shift the beat frequency away from the range frequency. The target speed and position can be determined using various techniques. One such technique involves extracting the Doppler frequency from the phase difference of the chirps within the chirp frame, while the range frequency provides the target position.

In cases where multiple targets are present in the field, a beat frequency signal will contain multiple f_b, one for each target. To separate the full set of tones (i.e. targets), a Fourier transform of the beat frequency signal can be performed, which is commonly referred to as range-FFT. To determine the velocity of the targets at a specific position, a second discrete Fourier transform can be conducted on the phasors of the chirp frame, also known as the Doppler-FFT. This process can be visualized as performing the FFT of the rows and columns of the radar data matrix, where rows represent the multiple beat frequency samples and columns represent the phasor samples (see Fig. 1).

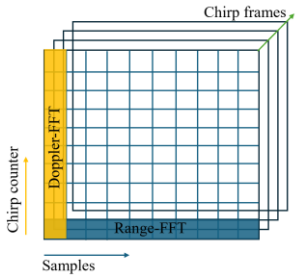

Fig. 1. Radar data matrix.

When the target has multiple moving parts the beat frequency, f_b^j,for a given position and the j moving part can be determined by Eq.9.

$$f_b^j = 2 \cdot \frac{v_r}{\lambda} + 2 \cdot \frac{\epsilon_j}{\lambda} + \frac{BW \cdot 2 \cdot d}{t_c \cdot c} = f_D + f_{MD} + f_R \quad (9)$$

Where ϵ_j is the change in velocity of the moving part j respecting the target main velocity v_r.

The resolution of both range and speed depends on the design parameters of the transmitted signal, as given by Eq.10 and Eq.11.

$$\delta R = \frac{c}{2 \cdot BW} \quad (10)$$

$$\delta V = \frac{\lambda}{2 \cdot T_f} \quad (11)$$

With T_f the period between chirp pulses.

The final step in the analysis of the radar echo signal involves the antenna array signals. When utilizing an antenna array to capture the reflected signal from a target that subtends a non-zero solid angle, there is a phase differences between the antennas due to their small spatial distance, $l_i(l_1$ and l_2 as it is described in Eq.12 and shown in Fig. 2). These phase differences can be observed as small increments in the phase of each auxiliary antenna with respect the phase of the reference antenna. Using these phases $\phi^{i}_{\text{Antenna}}$, the angle of arrival (AOA) of a target with respect to the normal direction of the antenna array θ is calculated using Eq.12.

$$\theta = arcsin\left(\frac{\lambda \phi^{i}_{Antenna}}{2\pi l_i}\right) \quad (12)$$

Eq.13 presents a relation between the phase differences obtained by two consecutive antennas relative to a common phase reference antenna.

$$\phi^1_{Antenna} = \frac{N}{M}\phi^2_{Antenna} + 2\pi\left(\frac{Nn_1 - Mn_2}{M}\right) \quad (13)$$

where $M, N \in \mathbb{N}$, M<N, and M, N have the greatest common divisor equal to 1, and $n1, n2 \in \mathbb{N}$ are two coefficients that represents the number of rotations above 2π in $\phi^{i}_{\text{Antenna}}$.

III. Radar Scheme

The foundational schematic of the FMCW radar is depicted in Fig. 2. The architecture employs a FPGA-based SDR, encompassing an up-conversion stage, a transmission branch, and three reception branches.

The SDR is implemented in a Xilinx FPGA platform and is optimized for real signal output at a rate of 6.144 GSPS. The S band signal produced exhibits a SINAD parameter of 70dB and is characterized by low jitter.

In the Analog Up-Conversion stage the conversion from S band to C band is implemented, for that a doubling factor C band multiplier from Mini-Circuit is employed. This conversion process significantly reduces the signal power, necessitating a 15dBm amplification stage prior to the passive local oscillators used in the RF Down-Conversion Stage. Subsequent to the amplification, a two-stage bandpass filter eliminates all harmonics induced by the multiplier and the amplifier's nonlinearity. The final component of the up-conversion stage comprises a 4-way splitter, also provided by Mini-Circuits. This component distributes the transmitting signal generated by the SDR along with the up-conversion stage, between the transmission branch and the three local oscillator inputs of the reception branches.

In the Power stage, a dual-stage amplification process is situated proximate to the antenna. The preamplifier is designed to offset the propagation losses encountered within the 3-meter 50Ω coaxial cable. A power amplifier for pulsed signals is chosen to ensure a minimum SNR of 9dB for detecting small targets (with -20 dB RCS values) at the system's maximum operational range of 350 meters.

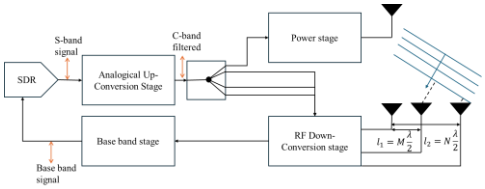

Fig. 2. 2D tracking MLBI radar architecture with 3 element phase interferometer as receiving antenna array.

This specific SNR threshold is imperative for the MLBI algorithm to accurately determine the AOA. In instances where the SNR falls below 9dB, although the range may be precisely estimated, the AOA calculation will suffer from erratic fluctuations among ambiguous angles due to the MLBI algorithm's imprecision.

The receiving antenna array consists of three symmetrical horn antennas. To enhance the SNR during detection, low-noise C-band amplifiers and C-band filters are incorporated within each antenna branch. Finally, the received signal is mixed with the transmitted signal, so a low frequency not chirped signal is obtained. This base band signal is filtered by a bandpass filter specifically tailored to the 400MHz bandwidth of the chirped signal, ensuring a flat frequency response across the entire region to preclude unwanted modulations on the baseband. This filter removes the harmonics produced by the mixing process and other out of band interferences. A base band amplifier is included to adjust the final voltage at the high rail of the Analog to Digital Converter (ADC) to utilize its full range.

The FPGA platforms play a pivotal role in data acquisition and execute the range-FFT in real time. To achieve this, a custom Vivado schematic has been developed, alongside multiple Hardware Description Language (HDL) custom blocks tailored for data rate synchronization with the Xilinx FFT Intellectual Property (IP) core. These platforms possess the capacity to handle high data rates in real time, which is crucial for achieving maximum range and optimal velocity resolution simultaneously. Additionally, the SDR board's low noise floor, approximately -120dBm, diminishes the need for high transmission power. This characteristic is significantly beneficial and represents a considerable advantage for radar applications, enhancing their efficiency and effectiveness in real-time target range and velocity determination. The integration of these elements underscores the FPGA platforms' robustness in processing and analysis, thereby ensuring high precision and reliability in radar operations.

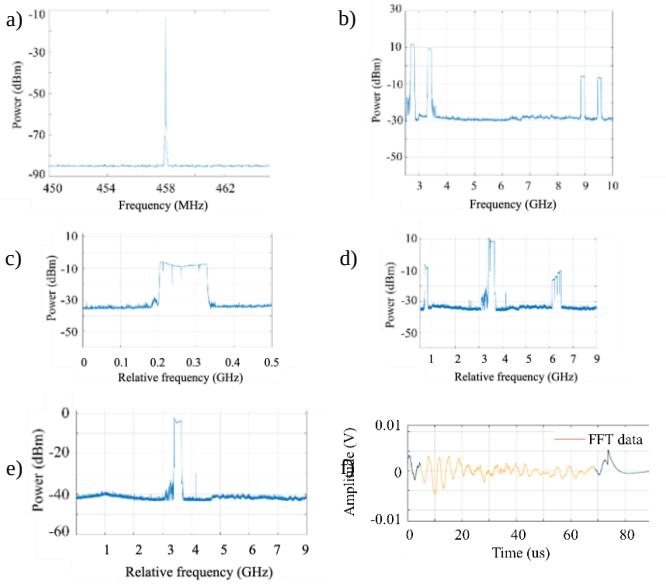

Fig. 3. ·Generated radar signals captured by an ESA a) Pure sinusoids tone, b) S-band signal, c) Filtered S band signal, d) C-band signal e) C-band filter signal f) Base band signal

In Figure 3a, a tone generated by the SDR system is observed, where the peak width represents the signal's jitter. As can be seen, its width is around 250kHz, which allows the final peaks in the received signal to also be of minimal thickness. This provides advantages in range resolution. In Figure 3b, the chirp generated by the same SDR system is seen, which correspond to the S-band signal position in Fig.2. Within Fig.3b, the effects of aliasing and mixing between the signal generated by the Digital to Analog Converter (DAC) and the internal Numerically Controlled Oscillator (NCO) of the SDR system can be observed. In the Fig.3c, a zoomed view of the chirp region of interest is presented, which will serve as a basis after its filtering for the generation of the C-band signal. This C-band signal can be seen in Fig. 3d. Harmonics resulting from its generation through the multiplication of the SDR signal also appear in it. These harmonics will be filtered out to yield the final signal that will be emitted. In Fig. 3e, the final signal is observable which corresponds to Fig.2 C-band filtered position. Note that the absolute frequency can be easily varied by altering the tone generated in the SDR. This last signal will be amplified for emission through a horn-type antenna.

Lastly, in Fig. 3f, the baseband signal collected through a cable, serving as an attenuation medium during system testing in the laboratory, is visible. Within this figure, a sinusoid whose frequency is proportional to the cable's length can be seen. This signal serves as an example of the Base band signal position in Fig.2.

IV. Experimental Results

The radar system underwent testing atop a university building. Fig. 4a displays the site of the testing and the positioning of the antennas. Fig. 4b reveals the interior of the enclosure housing the radar system, within which the FPGA utilized as an SDR system is visible.

The system's principal operational parameters include an azimuth and elevation aperture of 60 degrees, and a dynamic range higher than 50dB. Given these specifications, the system's theoretical range capability extends to 350 meters for targets exhibiting a RCS value of -20dB. To evaluate its performance, a Mavic 3 drone (shown in Fig. 4c) was deployed at an altitude of 120m, navigating upwards along a GNSS-specified trajectory illustrated in Fig. 5 as a blue trace.

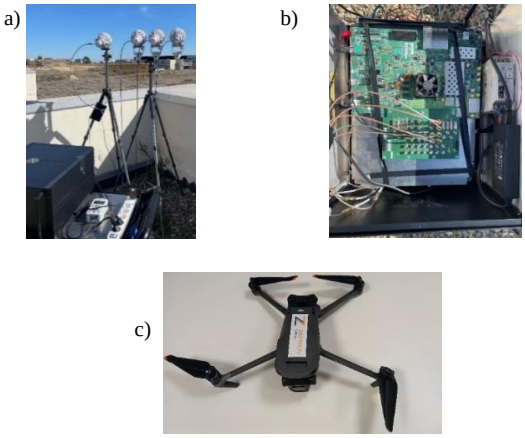

Fig. 4. ·a) Radar test system in the rooftop b) Top view of the open box which contains the radar c) DJI Mavic 3 drone.

In Fig.5 the values measured by the system can also be seen represented as an orange trace. Both traces match perfectly as it should after the system calibration process. The calibration process corrects the offset in angles due to fixed lags between FPGA channel and offset in position due different speed of the signal inside the cables.

Fig.6a shows, in a polar plot, the measured angles for the same trajectory. Fig. 6b represents the phase values measured by the system following the phase line (in blue) calculated by the MLBI algorithm.

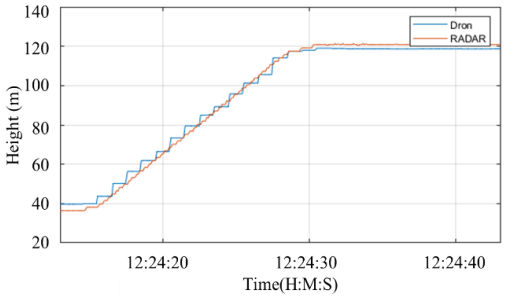

Fig. 5. ·Height measured by the radar (orange trace) compared to the height given by the IMU system of the drone (blue trace)

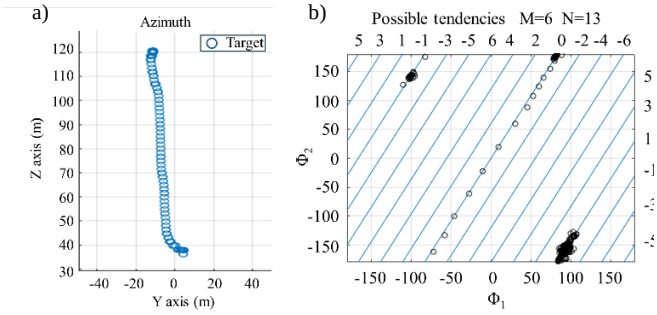

Fig. 6. a) Azimuth measurement of the drone in a vertical flight. b) phase values of the signal reflected by the drone along a vertical flight

Fig. 7 shows a round-trip drone flight 500m away from the radar location shown in Fig. 4a. It is represented in a waterfall plot base on the data measured by the system. The drone flight is the bell-shaped trace on the waterfall. The trace shows that the drone is clearly detected at distances up to 350m.

Due to the high quality of the signals obtained, the micro-Doppler characteristics can be observed and analyzed. With adequate velocity resolution, each target can be identified by its unique Doppler signal, which is a combination of the Doppler signals of the main body and the separately moving parts (the MDS).

Fig. 8 displays a measured micro-doppler signature of the drone. The main body of the drone is represented by the yellow bubble, while the vertical lines adjacent to it correspond to the propellers. It is worth noting that the distance between these lines varies depending on the speed of the drone. In the same figure, at the zero-velocity position, which appears as a yellow patch, corresponds predominantly to clutter, since this is static. In addition to the drone signal and the clutter, there are defects from the system that create soft vertical lines due to failures in data acquisition. These failures are attributed to system saturations, errors in acquiring UDP frames, or interference caused by external emitters.

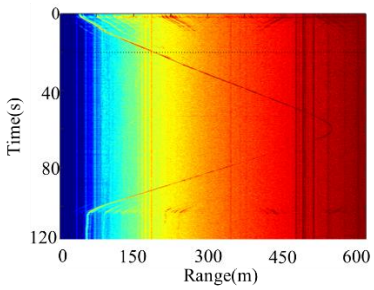

Fig. 7. ·Trace corresponding to a horizontal drone flight up to 500m.

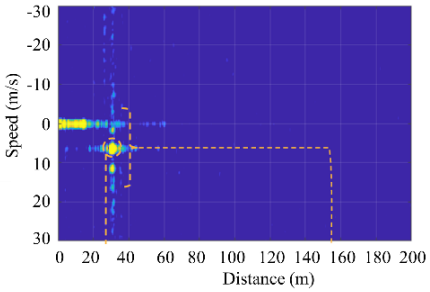

Fig. 8. · Micro-doppler signature of the drone.

V. Conclusions

In this study, the development of a C-band homodyne FMCW radar system utilizing SDR hardware and a three-element MLBI receiver is introduced for tracking and classifying low RCS targets up to a range of 350 meters. The basics of the radar design and the AOA estimation algorithm have been outlined. Furthermore, the radar system is capable of identifying the MD signature of targets, enabling classification through pattern recognition algorithms. These capabilities are achieved through the implementation of a homodyne architecture using commercial components. The phased array used in the system is also constructed from commercial antennas. Finally, the system was deployed in a field for empirical testing with a drone target to demonstrate its operational performance.

Acknowledgments

This work is part of the grant DIN2021-011740 financed by MCIN/AEI with DOI /10.13039/501100011033, and by INVESTIGO Program grant Z- 0034-INVESCS-22 by DGA.

References

[1] Merrill I. Skolnik, M.I. "*Introduction to Radar Systems",* Tata McGraw-Hill Education: New York, NY, USA, 2001.

[2] Zhengyu Peng, Changzhi Li, Roberto Gomez-Garcia, Jose-Maria Muñoz-Ferreras, "*Hardware development and applications of portable FMCW radars*". *DOI: 10.1049/SBRA531E_ch9*

[3] S.O. Piper, *"Homodyne FMCW radar range resolution effects with sinusoidal nonlinearities in the frequency sweep",DOI: 10.1109/RADAR.1995.522609*

[4] K. Stasiak and P. Samczynski, "FMCW radar implemented in SDR arquitecture using a USRP device" *DOI: 10.1109/SPS.2017.8053654*

[5] Liu, W., Weiss, S., 2010. *"Wideband Beamforming: Concepts and Techniques"*. John Wiley & Sons, UK. DOI 10.1002/9780470661178

[6] C. Schroeder, H. Rohling, "X-band FMCW radar system with variable chirp duration". *DOI:10.1109/RADAR.2010.5494425*

[7] Samiur Rahman, Duncan A. Robertson, "Radar *micro-Doppler signatures of drones and birds at K-Band and W-Band*". *DOI: 10.1038/s41598-018-35880-9*